eprints@whiterose.ac.uk
https://eprints.whiterose.ac.uk/

Synaptotagmin IV determines the linear Ca^{2+} dependence of vesicle fusion at auditory ribbon synapses

Stuart L Johnson[1], **Christoph Franz**[2], **Stephanie Kuhn**[3,7], **David N Furness**[4], **Lukas Rüttiger**[2], **Stefan Münkner**[3,5], **Marcelo N Rivolta**[1], **Elizabeth P Seward**[1], **Harvey R Herschman**[6], **Jutta Engel**[3,5], **Marlies Knipper**[2], and **Walter Marcotti**[1]

[1]Department of Biomedical Science, University of Sheffield, Sheffield, UK

[2]Department of Otolaryngology, Tübingen Hearing Research Centre, Laboratory of Molecular Physiology of Hearing, University of Tübingen, Tübingen, Germany

[3]Institute of Physiology II and Department of Otolaryngology, Tübingen Hearing Research Centre, University of Tübingen, Tübingen, Germany

[4]Institute of Science and Technology in Medicine, Keele University, Keele, UK

[5]Department of Biophysics, Saarland University, Homburg/Saar, Germany

[6]Department of Biological Chemistry, University of California Los Angeles Center for the Health Sciences, Los Angeles, California, USA

Abstract

Mammalian cochlear inner hair cells (IHCs) are specialized for the dynamic coding of continuous and finely graded sound signals. This ability is largely conferred by the linear Ca^{2+} dependence of neurotransmitter release at their synapses, which is also a feature of visual and olfactory systems. The prevailing hypothesis is that linearity in IHCs occurs through a developmental change in the Ca^{2+} sensitivity of synaptic vesicle fusion from the nonlinear (high order) Ca^{2+} dependence of immature spiking cells. However, the nature of the Ca^{2+} sensor(s) of vesicle fusion at hair cell synapses is unknown. We found that synaptotagmin IV was essential for establishing the linear exocytotic Ca^{2+} dependence in adult rodent IHCs and immature outer hair cells. Moreover, the expression of the hitherto undetected synaptotagmins I and II correlated with a high-order Ca^{2+} dependence in IHCs. We propose that the differential expression of synaptotagmins determines the characteristic Ca^{2+} sensitivity of vesicle fusion at hair cell synapses.

The exquisite temporal acuity of the mammalian auditory organ, which is essential for sound perception and localization, largely depends on the transfer characteristics of ribbon synapses in IHCs[1,2], the primary receptors of the mammalian cochlea. Ribbon synapses are

found in sensory receptors that respond to sustained and graded stimuli, such as those in the auditory and visual systems[3,4], and are believed to facilitate the coordinated release of synaptic vesicles[5,6]. Synaptic ribbons are specialized electron-dense organelles that tether a large number of vesicles at the cell's presynaptic active zones[4]. Neurotransmitter release at functionally mature sensory ribbon synapses (high-frequency IHCs and rod photoreceptors) depends linearly on Ca^{2+} influx[7-9], the effect of which is to broaden the cell's dynamic range to relay graded sound and light information to central synapses. In immature IHCs, neurotransmitter release shows a nonlinear (high order) dependence on Ca^{2+} (with a Ca^{2+} cooperativity of about 4) that is suited for encoding the spontaneous Ca^{2+}-driven action potential activity characteristic of these developing cells[7,9]. In contrast, exocytosis at immature outer hair cell (OHC) ribbon synapses, which do not fire spontaneous action potentials[10], depends linearly on Ca^{2+} (mouse[11], gerbil[12]). Although the function of ribbon synapses has been partially elucidated, the full identity of their molecular composition, including that of the proteins involved in determining the Ca^{2+} dependence of vesicle fusion, remains a major challenge[13,14]. Current models for hair cell ribbon synapses suggest that they lack some of the proteins found at conventional synapses[15], such as synaptophysins and the well-established Ca^{2+}-sensing triggers for vesicle fusion synaptotagmins I and II (Syts I and II), which are found throughout the CNS[16] and visual system[13]. In cochlear hair cells, the transmembrane protein otoferlin has been proposed, on the basis of an absence of Syts, to be the major Ca^{2+} sensor of synaptic vesicle fusion[11,17], although this view has been challenged[9,18]. More recently, it has been suggested that otoferlin, by interacting with the unconventional myosin VI, is involved in the transport of intracellular compartments to the IHC basolateral membrane (that is, replenishment of synaptic vesicles) and in the topographical organization of the presynaptic active zones[19]. Thus, synaptic vesicle fusion in mammalian hair cells could be controlled by Ca^{2+}-sensing proteins other than otoferlin.

Synaptotagmins are a large family of synaptic vesicle proteins that, among other functions, act as calcium regulators of exocytosis. They have a hierarchy of calcium affinities[20]. However, the function of most synaptotagmins in synaptic vesicle release is either unclear or varies depending on the cell type in which they are expressed[21-23]. One such synaptotagmin, synaptotagmin IV (Syt IV), is a unique, but ubiquitous, isoform that does not bind calcium in the C2A Ca^{2+}-sensing domain[20].

Syt IV is expressed in the adult mammalian cochlea[15]. The investigation of hair cells in Syt IV knockout mice[24] ($Syt4^{-/-}$) provides a unique opportunity to explore the role of this unusual synaptic protein in sensory neurotransmission. We found that Syt IV is required for establishing the linear exocytotic Ca^{2+} dependence characteristic of high-frequency adult IHCs and immature OHCs. We also found a correlation between the expression of Syt I and the high-order Ca^{2+} dependence in low-frequency adult and immature IHCs, whereas Syt II was only expressed in adult IHCs. This differential expression of Syts ensures that vesicle fusion at auditory ribbon synapses is finely tuned depending on the stage of development and the cells' frequency position.

RESULTS

We investigated the molecular identity and function of the Ca^{2+} sensor of exocytosis at cochlear hair cell ribbon synapses using *in situ* whole-cell patch-clamp recordings in near-physiological conditions (body temperature and physiological 1.3 mM extracellular Ca^{2+})[7,9], immunohistochemistry, *in situ* hybridization and transmission electron microscopy (TEM). The presynaptic function of hair cells in Syt IV knockout mice was assessed by measuring the increase in cell-membrane capacitance (ΔC_m), which is normally interpreted as a sign of neurotransmitter release.

Syt IV linearizes the exocytotic Ca^{2+} dependence of IHCs

At around the onset of hearing (postnatal day 12 (P12) in most rodents), the synaptic machinery of IHCs becomes more sensitive to Ca^{2+} over a physiologically relevant range, causing docked vesicles to be released linearly with increases in intracellular Ca^{2+} ([Ca^{2+}]$_i$)[7,9,12]. We found that exocytosis was not abolished in the absence of Syt IV, but the linear Ca^{2+} sensitivity of the mature mouse IHC synaptic machinery was not established. In adult Syt IV knockout IHCs, the maximal size of the Ca^{2+} current (I_{Ca}, -108 ± 6 pA, $n = 28$) and corresponding ΔC_m (20 ± 2 fF) was similar to that of control littermates (I_{Ca}, 110 ± 4 pA; ΔC_m, 21 ± 1 fF; $n = 27$) (Fig. 1a,b) and normal mice[7]. Despite this, the ΔC_m responses differed over the physiological range of membrane potentials (between about -70 to -11 mV; Fig. 1b). As a consequence, the exocytotic Ca^{2+} dependence, defined as the variation in ΔC_m as a function of I_{Ca} and displayed as a synaptic transfer function[7,9], was substantially less linear in the knockout (power of 3.1 ± 0.2, $n = 28$) than in control (power of 1.2 ± 0.1, $n = 27$; Fig. 1c) adult IHCs and was instead comparable to that of immature IHCs[7,9].

To confirm that the difference in exocytotic Ca^{2+} dependence seen between control and knockout IHCs (Fig. 1c) was not related to Ca^{2+} channel activation arising from differences in spatial coupling between Ca^{2+} channels and vesicle release sites[25], we investigated the intrinsic Ca^{2+} dependence of their exocytotic machinery[9]. For these experiments, any possible effect of Ca^{2+} channel activation on the exocytotic Ca^{2+} dependence[25] was eliminated by varying the size of I_{Ca} using different extracellular Ca^{2+} concentrations (in the physiological range of 1.3 mM) instead of voltage. We measured the resulting ΔC_m at a membrane potential at which the number of open Ca^{2+} channels was maximal and constant at each Ca^{2+} concentration (that is, at the peak of the I-V curve; Fig. 1b). The resulting synaptic transfer curves (control IHCs, power of 0.9 ± 0.1; knockout IHCs, 2.8 ± 0.1; Fig. 1d) matched those obtained when the membrane potential was varied (Fig. 1c), confirming that the difference that we observed in knockout IHCs was associated with an intrinsic change in their synaptic machinery. The altered Ca^{2+} dependence of exocytosis in adult Syt IV knockout IHCs was reflected in the significantly ($P < 0.001$) slower release kinetics of their readily releasable pool of vesicles compared with that of control cells (control, 20,306 $\pm$ 1,291 vesicles per s; knockout, 12,978 $\pm$ 1,304 vesicles per s; Fig. 1e), consistent with there being a higher-order exocytotic Ca^{2+} dependence in knockout cells. To exclude any possible correlation between ribbon shape and Ca^{2+} sensitivity of the synaptic machinery[9], we investigated the ribbon morphology using TEM (Fig. 1f). We found that the typical ellipsoid shape[26] and number[25] of synaptic ribbons in adult Syt IV knockout IHCs was normal (Fig. 1g).

As Syt IV is required for the linear exocytotic Ca^{2+} dependence in adult mouse IHCs, we hypothesized that it has no role in immature IHCs that show a high-order dependence on Ca^{2+} influx (mice[7], gerbils[9,12]). Such exocytotic Ca^{2+} cooperativity was confirmed in both control and Syt IV knockout immature IHCs (power of ~3: Fig. 2), confirming our hypothesis that Syt IV is unlikely to be involved in regulating synaptic transmission in immature IHCs.

The possible physiological effects associated with the altered exocytotic Ca^{2+} dependence in adult IHCs were tested by investigating hearing function of Syt IV knockout mice using auditory brainstem responses (ABRs), which reflect the activity of the afferent auditory pathway and IHCs. We found that knockout Syt IV mice had similar ABR thresholds to those of control mice (data not shown). However, it is possible that ABR thresholds are not sensitive enough to resolve the reduced exocytotic Ca^{2+} dependence in knockout IHCs. Alternatively, there may be some compensatory mechanism in the auditory pathway during the development of Syt IV knockout mice.

Syt IV determines the exocytotic Ca^{2+} dependence of OHCs

In the adult mammalian cochlea, the major role of OHCs is to enhance the sensitivity and frequency selectivity of hearing by active mechanical amplification[27]. Adult OHCs express functional Ca^{2+} channels[28] and have ribbon synapses, suggesting that they may be involved in transmitting sensory information to the brain.

At present, capacitance recordings of exocytosis in mature OHCs have not been achieved because of the large nonlinear capacitance (NLC) changes associated with their electromotile activity. However, ΔC_m measurements from early postnatal OHCs seem to be unaffected by NLC[11]. We verified this in P3–4 OHCs from Syt IV control mice (Supplementary Fig. 1). Similar to normal adult IHCs, exocytotic responses from immature OHCs depend linearly on Ca^{2+} (mouse[11], gerbil[12]). Therefore, our hypothesis was that an absence of Syt IV in OHCs would have an effect on the exocytotic Ca^{2+} dependence comparable to that observed in adult mouse IHCs (Fig. 1a–d). The Ca^{2+} dependence of neurotransmitter release in Syt IV knockout P3–4 OHCs was increased by a power of ~3 (Fig. 3), with similar maximal size of I_{Ca} and ΔC_m when compared to that of control cells (Fig. 3a,b), thus confirming our hypothesis.

Distribution of Syt IV in gerbil and mouse hair cells

The cellular distribution of Syt IV was investigated in whole-mount Mongolian gerbil and mouse cochleae (see Online Methods). Immunolabeling data were obtained from gerbils because, in our hands, the currently available Syt IV antibodies did not work on mice. However, the developmental changes in hair cell exocytotic Ca^{2+} dependence are better characterized in the gerbil[9,12] than in the mouse[7].

In the immature gerbil cochlea, we found that Syt IV was expressed in OHCs, but not in IHCs (Fig. 4a), confirming that the presence of Syt IV is specifically associated with the linear exocytotic Ca^{2+} dependence that is characteristic of OHCs (Fig. 4a). An additional benefit of using the gerbil, compared to the mouse, is that its cochlea has a low-frequency hearing range that extends well below a kHz (~0.1–60 kHz, from the apical to the basal region of the cochlea) compared to the mouse (~2–80 kHz), which is reflected in the properties of IHC neurotransmitter release[9]. Although apical-coil IHCs from the adult mouse (~3 kHz) have a linear exocytotic Ca^{2+} dependence[7], the gerbil has the advantage of having IHCs with either high-order (low-frequency apical region, ~0.3 kHz) or linear (high-frequency basal region, ~30 kHz) Ca^{2+} dependence in the same cochlea[9] (Fig. 4b,c). We found that Syt IV was expressed in basal, but not in apical, adult gerbil IHCs (Fig. 4b,c), where it was located throughout the cells, but tended to show a greater presence in the region of the presynaptic Ca$_V$1.3 Ca^{2+} channels (Fig. 4c). Thus, the presence/absence of Syt IV was directly correlated with the linear/high-order exocytotic Ca^{2+} dependence observed in auditory hair cells (Fig. 4). *In situ* hybridization experiments showed that Syt IV was also expressed at the IHC level in adult mice (Fig. 4d), which had a linear exocytotic Ca^{2+} dependence (Fig. 4d). These results are consistent with previous findings of its presence in the adult rat and guinea pig cochlea using reverse transcription PCR[15].

Syt IV IHCs have normal biophysical properties

We investigated the electrical properties of IHCs from Syt IV mice to determine whether the lack of Syt IV had additional effects on the normal function or development of these cells. The size of immature and adult K$^+$ currents recorded from knockout IHCs was similar to those in littermate controls (Fig. 5a–f). Moreover, all of the other biophysical properties, including resting membrane potentials and linear leak conductance, did not differ between control (P5, $n = 6$; P28, $n = 7$) and knockout (P5, $n = 8$; P29, $n = 7$) Syt IV IHCs (Supplementary Tables 1 and 2). These findings, together with the normal appearance of

ribbons in adult IHCs (Fig. 1f,g), indicate that the abnormal exocytotic Ca^{2+} dependence in Syt IV knockouts (Fig. 1a-e) was not a result of a general failure in IHC maturation or of cell deterioration.

The maturation of the synaptic machinery in IHCs (from high-order Ca^{2+} dependence to a linear relation) is likely to be controlled by their spontaneous Ca^{2+}-dependent action potential activity[29] before the onset of hearing (P12). The similar spiking activity seen in both immature control (average frequency, 2.3 ± 0.6 Hz, $n = 8$, P5) and Syt IV knockout (1.9 ± 0.9 Hz, $n = 4$, P5) IHCs (Fig. 5g,h) excludes any indirect role for Syt IV in the developmental linearization of Ca^{2+}-dependent exocytosis in these cells. The absence of Syt IV in immature IHCs (Fig. 3a) provides compelling support for this. Moreover, spontaneous action potentials do not occur in immature OHCs (when using near physiological recording conditions[10,12]), arguing against any activity-dependent influence of Syt IV in the developmental linearization of exocytosis in auditory hair cells in general.

Alternatively, Syt IV could have a more immediate (as opposed to a developmental role), but still indirect, influence on IHC synaptic transmission. Such a role has been shown in hippocampal neurons, where Syt IV inhibits presynaptic vesicle exocytosis by limiting the retrograde postsynaptic release of brain-derived neurotrophic factor (BDNF)[21], a neuromodulator that enhances neurotransmission and synaptic plasticity. However, a retrograde regulatory role for Syt IV is unlikely to occur in auditory hair cells, as K-252a, a blocker of neurotrophin signaling mediated by the BDNF receptor trkB, did not affect exocytosis in control IHCs (Supplementary Fig. 2). Moreover, in contrast with the CNS, Syt IV in hair cells would need to promote vesicle release, rather than inhibit it, to account for the observed increase in Ca^{2+} efficiency (Fig. 1c). A retrograde signaling mechanism for Syt IV would probably be too slow to affect the extremely rapid responses characteristic of sensory hair cells.

These findings corroborate the specific and direct role of Syt IV in establishing the linear relation between exocytosis and Ca^{2+} entry in auditory hair cells, the physiological importance of which would be to broaden the range of intracellular Ca^{2+} that regulates neurotransmitter release. However, an additional Ca^{2+} sensor has to be present to promote the high-order Ca^{2+} dependence of exocytosis observed in immature IHCs and in Syt IV knockout hair cells.

Syt I and II expression in IHCs

A previous study of the adult cochlea suggested that synaptotagmins I and II are not expressed in hair cells[15] and it is instead believed that the transmembrane protein otoferlin is the only determinant of the exocytotic Ca^{2+} sensitivity at these ribbon synapses[11,17]. We found that in immature mouse IHCs, which have high-order exocytotic Ca^{2+} dependence (Fig. 2c), Syt I was expressed and colocalized with otoferlin (Fig. 6a). In contrast, Syt I was not expressed in immature OHCs that showed otoferlin labeling (Fig. 6a) and had a linear exocytotic Ca^{2+} dependence (Fig. 3). In the adult cochlea, Syt I expression was only observed in the efferent terminals contacting afferent fibers below IHCs (Fig. 6b), as indicated by its specific colocalization with the efferent marker VAMP2. We observed identical staining patterns for Syt I and otoferlin in Syt IV knockout mice (data not shown). In the adult gerbil, Syt I was expressed in apical-coil, but not in basal-coil, IHCs (Supplementary Fig. 3), providing additional evidence for the direct correlation between the presence of Syt I and the high-order exocytotic Ca^{2+} dependence.

We investigated the possible involvement of Syt I in IHC synaptic transmission using adult hypothyroid rats[18], an animal model in which hair cells have immature characteristics and, more importantly, do not express otoferlin[18]. In these rats, IHCs retained Syt I expression

(Fig. 6c) and had an exocytotic Ca^{2+} dependence that resembled that of immature IHCs (Fig. 6d). The absence of otoferlin (data not shown) suggests that, similar to the rod photoreceptor[13], the Ca^{2+} sensor Syt I is involved in vesicle fusion in IHCs exhibiting a high-order exocytotic Ca^{2+} dependence. When we tested hypothyroid IHCs for vesicle pool refilling[9,12], using repetitive voltage steps to −11 mV, a time-dependent decline in the cumulative ΔC_m became evident (significant at $P < 0.0001$ compared with that of immature control IHCs; Fig. 6e), indicating that in the absence of otoferlin vesicle replenishment was impaired.

We also investigated the expression of Syt II, the other main Ca^{2+} sensor of exocytosis, in the cochlea using immunolabeling. The specificities of the Syt I and Syt II antibodies were verified by pre-incubating each of them with both antigenic peptides (Supplementary Fig. 4). Under our experimental conditions, Syt II was not detected in immature hair cells, but was located close to the efferent terminal region (Fig. 7a). In contrast, Syt II was expressed in adult IHCs (Fig. 7b), where it is likely to be responsible for the high-order Ca^{2+} dependence seen in these cells in Syt IV knockout mice. In the adult gerbil, Syt II was expressed in both apical and basal IHCs (Supplementary Fig. 3), although its expression was much weaker in the former.

DISCUSSION

Ca^{2+} sensors for exocytosis at auditory ribbon synapses

All chemical synapses include a mechanism for the Ca^{2+}-dependent fusion of docked vesicles. However, most sensory cells differ from spiking neurons because they generate graded receptor potentials, have to sustain exocytosis at much higher rates and must be able to transmit sensory information across a wide dynamic range[3,4]. These characteristics are thought to be conferred by synaptic ribbons[4,13] and the ability of mature sensory cells to fuse docked vesicles to the plasma membrane linearly with Ca^{2+} influx[7,8]. In high-frequency IHCs (kHz range), this linearization supersedes the high-order Ca^{2+}-dependent synaptic machinery of immature spiking cells at around the onset of hearing[7,12].

The absence of exocytosis in cochlear hair cells of otoferlin-deficient mice[11,17] (vestibular hair cells of these animals do show exocytosis[30]), together with the apparent lack of synaptotagmins I and II in the adult cochlea[15], led to the suggestion that the transmembrane protein otoferlin was the major Ca^{2+} sensor of vesicle release in auditory hair cells. However, otoferlin is not required for vesicle fusion[18] or for determining the high-order Ca^{2+} dependence of neurotransmitter release (Fig. 6d) and appears to have a different role in cochlear[11,17] and vestibular hair cells[30]. Recent findings have shown that otoferlin seems to be involved in setting the linear exocytotic Ca^{2+} dependence in vestibular hair cells[30]. In the cochlea it is unlikely to work similarly, as we found that otoferlin was present in hair cells from Syt IV knockout mice (data not shown) and apical-coil IHCs from the adult gerbil[9], both of which did not show the linear relation. Moreover, in the auditory system, otoferlin is expressed in all hair cells, irrespective of whether they show a linear or high-order exocytotic Ca^{2+} dependence[9,12]. Nevertheless, otoferlin appears to be essential for the topographical organization of the presynaptic active zones in cochlear hair cells[19] and our results suggest that it is involved in synaptic vesicle replenishment (Fig. 6e).

We found that synaptotagmins I, II and IV were differentially expressed in hair cells during cochlear development and correlated with the Ca^{2+} sensitivity of neurotransmitter release (Supplementary Fig. 5). Synaptotagmins are a large family of synaptic vesicle proteins that, through their C2 domains, bind phospholipids, interact with other known synaptic proteins and, in most cases, bind Ca^{2+} directly[20]. Although Ca^{2+} binding to the C2B domain (but not to the C2A domain) of Syt I is essential for vesicle fusion, Ca^{2+} binding to the C2A domain

determines the Ca^{2+} cooperativity of exocytosis[31]. As such, synaptotagmins are known to be the primary regulators of neurotransmitter release[16].

Role of Syt IV in hair cell synaptic transmission

The function of Syt IV is currently unclear, as its C2A domain is unable to bind Ca^{2+} (ref. 20). *Synaptotagmin IV* is an immediate early gene induced by chronic activity[32] and is thought to have a neuroprotective effect by decreasing evoked neurotransmission in *Drosophila*[22]. As with Syts I and II, Syt IV is ubiquitously expressed throughout the nervous system. Its role in vesicle fusion remains controversial, with many conflicting findings. Some reports question its involvement in synaptic transmission[33], whereas others suggest that it either promotes[23] or inhibits[21,22] exocytosis.

In the mammalian cochlea, we found that Syt IV has a direct role in synaptic transmission by establishing the linear relation between Ca^{2+} entry and vesicle release (Supplementary Fig. 5), which consequently enhances the Ca^{2+} efficiency of the synaptic machinery over the physiological range of Ca^{2+} concentrations. The correlation between Syt IV expression and a linear synaptic Ca^{2+} dependence suggests that such a relation is unlikely to arise from a closer spatial coupling between Ca^{2+} channels and release sites. This was verified by comparing the degree of colocalization between Ca^{2+} channels and docked vesicles using different concentrations of the Ca^{2+} chelator BAPTA in immature (high-order exocytotic Ca^{2+} dependence) and adult (linear) mouse IHCs (Supplementary Fig. 6). A recent study of Syt I showed that Ca^{2+} binding in the C2A domain regulates Ca^{2+} binding to the C2B domain and consequently determines the Ca^{2+} cooperativity of vesicle fusion[31]. Therefore, the linear exocytotic Ca^{2+} dependence in hair cells expressing Syt IV could arise from the inability of this isoform to bind Ca^{2+} in the C2A domain.

The linear synaptic Ca^{2+} dependence is a common feature of sensory cells in the auditory, visual and olfactory systems and seems to be essential for allowing cells to represent graded physiological stimuli and to extend the dynamic range over which they operate[7,8,34]. Therefore, Syt IV could potentially have a similar role at linear synapses in other sensory systems[8,34]. Synaptotagmin IV is required for neuro-secretion from pituitary nerve terminals where it has a similar overall effect by broadening the range of Ca^{2+} controlling exocytosis[35]. In this case, however, broadening is achieved by inhibiting release at low Ca^{2+} levels and enhancing it at high levels[35], which is opposite to our findings from auditory hair cell synapses. Although Syt IV is able to functionally replace Syt I in some systems by promoting exocytosis[23] via the interaction of Ca^{2+} with its C2B domain[36,37], it is likely that the different functional roles observed for Syt IV in exocytosis result from its interaction with additional Ca^{2+} sensing proteins such as other Syt isoforms, providing a unique role for Syt IV in tuning/regulating cell physiological responses.

Auditory hair cells express Syts I and II

Detailed genetic and biochemical investigations have established Syts I and II as the main Ca^{2+} sensors[38,39] determining the high-order Ca^{2+} dependence of neurotransmitter release at central synapses[40], a role that has been ascribed to the Ca^{2+}-binding properties of their C2A domain[20,31]. In mammalian hair cells, Syt I expression was solely correlated with a high-order exocytotic Ca^{2+} dependence. Syt II was exclusively expressed in adult IHCs (Supplementary Fig. 5), where it is likely to be responsible for the residual high-order relation in Syt IV knockout mice.

A conserved property among synaptotagmin isoforms is their ability to form clusters of hetero-oligomers[41]. The simultaneous expression of synaptotagmins with different Ca^{2+}-binding affinities could thus generate a wide range of synaptic Ca^{2+} sensitivities[20].

Synaptotagmin IV has been shown to hetero-oligomerize with Syt I[22,42], but this interaction, which is found throughout the CNS, has been associated with an inhibitory effect on synaptic vesicle release in *Drosophila*[22]. We found that this inhibitory effect also occurred when we overexpressed Syt IV in mammalian chromaffin cells that endogenously express Syt I (Supplementary Fig. 7). This provides a possible explanation for the absence of Syt I from hair cells showing a linear Ca^{2+} dependence (that is, those with an enhanced exocytotic Ca^{2+} efficiency).

Reconstitution experiments in neurons and chromaffin cells indicate that Syts I and II have very similar functions as Ca^{2+} sensors for triggering fast secretion of readily releasable vesicles, albeit with different kinetics[43,44]. Notably, both Syts I and II exhibited a binding stoichiometry of five Ca^{2+} ions per molecule, micromolar Ca^{2+} affinity, and bound phospholipids and SNARE proteins. This suggests that the switch from Syt I to Syt II must be important for another isoform-specific property, such as the nature of their interaction with other Syts. The interaction of Syt II with IV could lead to an increased exocytotic Ca^{2+} efficiency that is characteristic of a linear exocytotic Ca^{2+} dependence. Moreover, Syt II is able to trigger vesicle release faster than Syt I[45], which would be essential for sustaining the high temporal acuity that is characteristic of these adult cells. Although hetero-oligomerization between Syts II and IV has yet to be demonstrated, the similarity between Syts I and II suggests that it is likely. An additional or alternative hypothesis is that Syt IV could reduce the number of Ca^{2+}-dependent steps involved in vesicle release by promoting the kiss-and-run mode of exocytosis[36] as opposed to full fusion, although there is no evidence for such a mechanism at hair-cell ribbon synapses. Immature OHCs express neither of the two classical synaptotagmins, indicating that an additional and as yet unidentified Ca^{2+} sensor, such as another synaptotagmin isoform, must be present in these cells.

The maturation of the mammalian cochlea is thought to be driven by spontaneous Ca^{2+} action-potential activity in immature IHCs[29], as occurs in other parts of the nervous system[46]. Therefore, the differential developmental expression of synaptotagmins could be controlled by this early electrical activity[47]. This possibility is likely given the observation that abnormal firing activity in immature IHCs from SK2 (small conductance Ca^{2+}-activated K^+ channel) knockout mice has been shown to prevent the normal developmental linearization of the exocytotic Ca^{2+} dependence[29].

METHODS

Methods and any associated references are available in the online version of the paper at http://www.nature.com/natureneuroscience/.

ONLINE METHODS

Electrophysiology

Apical coil IHCs ($n = 122$) and OHCs ($n = 47$) from synaptotagmin control (*Syt4*^{+/+} and *Syt4*^{+/−}) and knockout (*Syt4*^{−/−}) mice[24] were studied in acutely dissected organs of Corti from P3 to P36, where the day of birth was P0. A few experiments were also performed on rat IHCs (P4–18, $n = 26$). All animals used for electrophysiology and TEM and some of those used for immunolabeling experiments were killed by cervical dislocation in the UK in accordance with UK Home Office regulations. Cochleae were dissected in normal extracellular solution (135 mM NaCl, 5.8 mM KCl, 1.3 mM $CaCl_2$, 0.9 mM $MgCl_2$, 0.7 mM NaH_2PO_4, 5.6 mMD-glucose, 10 mM HEPES-NaOH, 2 mM sodium pyruvate, amino acids and vitamins, pH 7.5). All recordings were performed near body temperature (35–37 °C). Command voltage and current protocols were applied and data acquired using pClamp software and a Digidata 1322A (Molecular Devices) and analyzed with Origin (Origin Lab).

Electrophysiological experiments were carried out using the Optopatch amplifier (Cairn Research).

Recordings of K^+ currents and voltage responses were performed using a K^+-based intracellular solution (131 mM KCl, 3 mM $MgCl_2$, 1 mM EGTA-KOH, 5 mM Na_2ATP, 5 mM HEPES-KOH and 10 mM sodium phosphocreatine, pH 7.3). Current and voltage responses were filtered at 2.5 kHz (8-pole Bessel), sampled at 5 kHz and stored on computer for off-line analysis.

The intracellular solution used for exocytosis measurements contained 106 mM cesium glutamate, 20 mM CsCl, 3 mM $MgCl_2$, 1 mM EGTA-CsOH, 5 mM Na_2ATP, 0.3 mM Na_2GTP, 5 mM HEPES-CsOH and 10 mM sodium phosphocreatine (pH 7.3). The exocytosis of synaptic vesicles[7,9] was measured using a 4-kHz sine wave (13-mV r.m.s.) applied to hair cells from −81 mV and was interrupted for the duration of the voltage step. The capacitance signal from the Optopatch was amplified (50×), filtered at 250 Hz, sampled at 5 kHz and measured by averaging the C_m traces after the voltage step (around 200 ms) and subtracting from pre-pulse baseline. ΔC_m was recorded in the presence of the K^+ channel blockers TEA (30 mM), 4-AP (15 mM) and either apamin (300 nM) or linopirdine (80–100 μM)[7,9]. Membrane potentials were corrected for the voltage drop across the series resistance R_s (mice, 5.5 ± 0.1 MΩ, $n = 169$; rats, 6.2 ± 0.2 MΩ, $n = 26$) and a liquid junction potential of −11 mV, measured between electrode and bath solutions. All animals were genotyped as described previously[24]. The rate of vesicle fusion (Fig. 1e) was obtained by measuring ΔC_m in response to depolarizing voltage steps to −11 mV, from the holding potential of −81 mV, of varying duration (2 to 50 ms). This protocol allows for the isolation of the readily releasable pool when performing the recordings at body temperature and using 1.3 mM extracellular Ca^{2+} (ref. 9). The size and release kinetics of the isolated readily releasable pool was approximated by fitting the data points from each individual cell using a single exponential function. The number of vesicles was estimated using a conversion factor of 37 aF per vesicle[49]. Synaptic transfer functions (see Figs. 1c,d, 2c, 3c and 6d) were fitted using a power function

$$\Delta C_m = c I_{Ca}^N \quad 1$$

where c is a scaling coefficient and the power is N. The average N values reported are from fits to all individual cells tested.

Statistical analysis

Statistical comparisons of means were made by Student's two-tailed t test or, for multiple comparisons, analysis of variance, usually one-way ANOVA followed by the Tukey test. Two-way ANOVA, followed by the Bonferroni test, was used to compare datasets from two different conditions. Mean values are shown ± s.e.m. where $P < 0.05$ indicates statistical significance.

Immunostaining

Cochleae from NMRI mice, Wistar rats (Charlse Rivers) and Syt IV control and knockout mice were used to prepare cryosections for immunofluorescence microscopy and processed as previously described[19]. Briefly, cochleae were dissected and fixed for 2 h with 2% paraformaldehyde (wt/vol), decalcified, embedded in Tissue-Tek optimal cutting temperature compound (Sakura Finetek) and cryosectioned at a thickness of 10 μm. Sections were embedded with Vectashield mounting medium with DAPI (Vector Laboratories). Antibodies to synaptotagmin I or II (rabbit, Synaptic Systems, diluted 1:50), otoferlin (mouse, Abcam, 1:100) and synaptobrevin2/VAMP2 (mouse: Synaptic Systems,

1:300) were used for cryosection preparations. Immunofluorescence staining for synaptotagmin IV was performed on whole-mount immature and adult Mongolian gerbil cochleae because, in our hands, the current commercially available Syt IV antibodies did not work on mice, rats or on cryosections. Gerbil cochleae were perfused with 2% paraformaldehyde for 15 min followed by $1 \times$ phosphate-buffered saline (PBS). The whole organs of Corti were dissected out in $1 \times$ PBS, mounted on slides using BD Cell-Tak Cell and Tissue Adhesive (BD Bioscience) and immunostained with synaptotagmin IV (mouse, Abcam, 1:50) and Ca^{2+} channel $Ca_V1.3$ (rabbit, Alomone Labs, 1:50) antibodies. Animals processed in Germany were killed by CO_2 asphyxiation or cervical dislocation in accordance with the ethical guidelines approved by the University of Tübingen and the Tierschutzgesetz (Germany).

Primary antibodies were detected with Cy3-conjugated (Jackson ImmunoResearch Laboratories) or Alexa Fluor 488–conjugated secondary antibodies (Molecular Probes). Sections and whole-mount preparations were viewed using an Olympus AX70 microscope equipped with epifluorescence illumination. Images were acquired using a CCD camera and analyzed with cell^F software (OSIS). For the whole-mount preparation, cochleae were imaged over a distance of several μm with the coverage of the IHC synaptic region in an image-stack along the z axis (z stack) and three-dimensionally deconvoluted using cell^F's RIDE module with the Nearest Neighbor algorithm (OSIS). Figure 4a–c shows composite images, which represent the maximum intensity projection over all layers of the z stack.

Immunostaining was also performed on Syt IV and NMRI mice (immature: NMRI, $n = 3$, Syt IV, control $n = 2$, Syt IV, knockout $n = 2$; adult: NMRI, $n = 2$, Syt IV control, $n = 3$, Syt IV knockout, $n = 3$), rats (immature: control, $n = 2$, hypothyroid, $n = 2$; mature: control, $n = 11$, hypothyroid, $n = 4$) and gerbils (immature, $n = 2$; adult, $n = 3$). Hypothyroidism in rats was induced by treatment with methyl-mercapto-imidazol as described previously[18]. Although the peptide for Syt IV was not available, its possible cross-reaction with Syt I and Syt II was excluded, as apical gerbil IHCs expressed both the Syt I and II (Supplementary Fig. 3), but not Syt IV (Fig. 4b).

Synaptotagmin IV riboprobe synthesis and whole-mount *in situ* hybridization

A PCR fragment of 898 base pairs was amplified from rat cochlear cDNA using oligonucleotide primers (Syt IV forward, 5′-GCC TAA CCT TTC CCT GCA CCT TGA-3′; Syt IV reverse, 5′-TCT GAA AGG GGA TCC CGA AAT GAG-3′), cloned using TOPO TA Cloning kit (Invitrogen), sequenced and reversely transcribed using DIG-RNA labeling mix (Roche). Complementary strands (antisense) were prepared by linearizing the plasmid with *Hin*dIII and transcribing the template from T7 promoter sites. Noncomplementary strands (sense) were prepared with NotI followed by transcription from the SP6 promoter site. The transcripts were precipitated in ethanol and re-suspended in 1 part hybridization buffer (Amersham), 1 part RNase-free H_2O and 2 parts deionized formamide (AppliChem).

Whole-mount *in situ* hybridization with Syt IV riboprobes was performed on adult mouse cochleae (>P30, NMRI, $n = 3$) fixed with 2% paraformaldehyde for 30 min followed by dehydration in 100% methanol overnight at −20 °C. After rehydration and digestion with proteinase K (2 μg ml^{-1}) at 37 °C for 3 min, cochleae were postfixed in 2% paraformaldehyde for 15 min at ~21 °C and washed with PBS containing 0.1% Tween 20 (vol/vol). Cochleae were prehybridized in the hybridization buffer overnight at 60 °C and then incubated for 3 h with hybridization buffer containing the riboprobes (antisense and sense, 1:300). They were then washed in $2 \times$ SSC (300 mM sodium chloride, 30 mM sodium citrate, pH 7.0) and $0.2 \times$ SSC at 60 °C. Cochleae were incubated for 2 h with a blocking reagent (1:10, Roche), which was followed by an overnight incubation with anti-Digoxigenin-AP Fab fragments solution (Roche) at 4 °C. Nitroblue tetrazolium salt (Sigma)

and 5-bromo-4-chloro-3-indolyl phosphate (Sigma) solutions were applied to the cochleae for up to 5 h until satisfactory staining was achieved. After stopping this reaction by washing cochleae with PBS containing 0.1% Tween 20 and ethanol (95%), we dissected cochleae and mounted pieces of the organ of Corti on slides.

TEM

Cochleae from P26 Syt IV control and knockout mice were prepared for TEM by perfusion with 2.5% glutaraldehyde (vol/vol) in 0.1 M sodium cacodylate buffer and were immersed for 2 h in the same fixative. They were then washed and postfixed in 1% osmium tetroxide (wt/vol) in the same buffer, decalcified for 72 h in 5 mM EGTA and embedded in Spurr's resin as described previously for cochlear segments[50]. The cochlea was sectioned in a plane transverse to the modiolus through the apical coil. Serial semi-thin, 400-nm-thick sections were cut and mounted on grids coated with a formvar film and examined unstained in a JEOL 1230 transmission electron microscope. Digital images of each IHC were acquired from up to 30 serial sections from the base to the nucleus and the numbers of synaptic ribbons were counted in four control (from one control mouse) and three knockout hair cells (from two mice). Ultrathin sections were also cut onto 200-mesh copper grids and stained with uranyl acetate and lead citrate before examination for synaptic structure in the TEM.

Chromaffin cell electrophysiology

Isolated adult bovine chromaffin cells were re-suspended at a density of 10^7 cells per 800 μl in growth media; 800 μl of the cell suspension was mixed with 25 μg cDNA (pEGFP Clontech, with or without pDNA3.1 encoding mouse Syt IV, Addgene) in a 1.5-ml micro-centrifuge tube. For co-transfections the amount of each cDNA used was 12.5 μg. The cells were incubated with the DNA for 5 min to allow binding of the DNA to the cell surface and were then transferred to a 4-mm electroporation cuvette for mammalian cells (Flowgen). Cells were electroporated using an exponential decay pulse type on either a Gene Pulser II or Gene Pulser XCell (both Bio-Rad). The cuvette was placed into the electroporation chamber and one pulse set at 250 V and 1,000 μF was applied. Cells were then rapidly transferred into 2 ml of fresh, pre-warmed media and plated on collagen-coated coverslips for experiments. The following day, fresh media was added to the cells. Electroporated cells were typically left for at least 48 h before experiments were carried out. Stimulus-secretion coupling in these cells (Supplementary Fig. 7) was quantified by combining measurements of I_{Ca} and ΔC_m as described above.

References

49. Lenzi D, Runyeon JW, Crum J, Ellisman MK, Roberts WM. Synaptic vesicle populations in saccular hair cells reconstructed by electron tomography. J. Neurosci. 1999; 19:119–132. [PubMed: 9870944]

50. Furness DN, Hackney CM. Cross-links between stereocilia in the guinea pig cochlea. Hear. Res. 1985; 18:177–188. [PubMed: 4044419]

Supplementary Material

Refer to Web version on PubMed Central for supplementary material.

Acknowledgments

References

1. Fuchs PA. Time and intensity coding at the hair cell's ribbon synapse. J. Physiol. (Lond.). 2005; 566:7–12. [PubMed: 15845587]

2. Moser T, Neef A, Khimich D. Mechanisms underlying the temporal precision of sound coding at the inner hair cell ribbon synapse. J. Physiol. (Lond.). 2006; 576:55–62. [PubMed: 16901948]

3. Juusola M, French AS, Uusitalo RO, Weckström M. Information processing by graded-potential transmission through tonically active synapses. Trends Neurosci. 1996; 19:292–297. [PubMed: 8799975]

4. Sterling P, Matthews G. Structure and function of ribbon synapses. Trends Neurosci. 2005; 28:20–29. [PubMed: 15626493]

5. Glowatzki E, Fuchs PA. Transmitter release at the hair cell ribbon synapse. Nat. Neurosci. 2002; 5:147–154. [PubMed: 11802170]

6. Singer JH, Lassová L, Vardi N, Diamond JS. Coordinated multivesicular release at a mammalian ribbon synapse. Nat. Neurosci. 2004; 7:826–833. [PubMed: 15235608]

7. Johnson SL, Marcotti W, Kros CJ. Increase in efficiency and reduction in Ca^{2+} dependence of exocytosis during development of mouse inner hair cells. J. Physiol. (Lond.). 2005; 563:177–191. [PubMed: 15613377]

8. Thoreson WB, Rabl K, Townes-Anderson E, Heidelberger R. A highly Ca^{2+}-sensitive pool of vesicles contributes to linearity at the rod photoreceptor ribbon synapse. Neuron. 2004; 42:595–605. [PubMed: 15157421]

9. Johnson SL, Forge A, Knipper M, Münkner S, Marcotti W. Tonotopic variation in the calcium dependence of neurotransmitter release and vesicle pool replenishment at mammalian auditory ribbon synapses. J. Neurosci. 2008; 28:7670–7678. [PubMed: 18650343]

10. Marcotti W, Kros CJ. Developmental expression of the potassium current $I_{K,n}$ contributes to maturation of the mouse outer hair cells. J. Physiol. (Lond.). 1999; 520:653–660. [PubMed: 10545133]

11. Beurg M, et al. Calcium- and otoferlin-dependent exocytosis by immature outer hair cells. J. Neurosci. 2008; 28:1798–1803. [PubMed: 18287496]

12. Johnson SL, Franz C, Knipper M, Marcotti W. Functional maturation of the exocytotic machinery at gerbil hair cell ribbon synapses. J. Physiol. (Lond.). 2009; 587:1715–1726. [PubMed: 19237422]

13. Lenzi D, von Gersdorff H. Structure suggests function: the case for synaptic ribbons as exocytotic nanomachines. Bioessays. 2001; 23:831–840. [PubMed: 11536295]

14. Glowatzki E, Grant L, Fuchs PA. Hair cell afferent synapses. Curr. Opin. Neurobiol. 2008; 18:389–395. [PubMed: 18824101]

15. Safieddine S, Wenthold RJ. SNARE complex at the ribbon synapses of cochlear hair cells: analysis of synaptic vesicle- and synaptic membrane-associated proteins. Eur. J. Neurosci. 1999; 11:803–812. [PubMed: 10103074]

16. Südhof TC. The synaptic vesicle cycle. Annu. Rev. Neurosci. 2004; 27:509–547. [PubMed: 15217342]

17. Roux I, et al. Otoferlin, defective in a human deafness form, is essential for exocytosis at the auditory ribbon synapse. Cell. 2006; 127:277–289. [PubMed: 17055430]

18. Brandt N, et al. Thyroid hormone deficiency affects postnatal spiking activity and expression of Ca^{2+} and K^+ channels in rodent inner hair cells. J. Neurosci. 2007; 27:3174–3186. [PubMed: 17376979]

19. Heidrych P, et al. Otoferlin interacts with myosin VI: implications for maintenance of the basolateral synaptic structure of the inner hair cell. Hum. Mol. Genet. 2009; 18:2779–2790. [PubMed: 19417007]

20. Südhof TC. Synaptotagmins: why so many? J. Biol. Chem. 2002; 277:7629–7632. [PubMed: 11739399]

21. Dean C, et al. Synaptotagmin-IV modulates synaptic function and long-term potentiation by regulating BDNF release. Nat. Neurosci. 2009; 12:767–776. [PubMed: 19448629]

22. Littleton JT, Serano TL, Rubin GM, Ganetzky B, Chapman ER. Synaptic function modulated by changes in the ratio of synaptotagmin I and IV. Nature. 1999; 400:757–760. [PubMed: 10466723]

23. Zhang Q, Fukuda M, Van Bockstaele E, Pascual O, Haydon PG. Synaptotagmin IV regulates glial glutamate release. Proc. Natl. Acad. Sci. USA. 2004; 101:9441–9446. [PubMed: 15197251]

24. Ferguson GD, Anagnostaras SG, Silva AJ, Herschman HR. Deficits in memory and motor performance in synaptotagmin IV mutant mice. Proc. Natl. Acad. Sci. USA. 2000; 97:5598–5603. [PubMed: 10792055]

25. Brandt A, Khimich D, Moser T. Few $Ca_V1.3$ channels regulate the exocytosis of a synaptic vesicle at the hair cell ribbon synapse. J. Neurosci. 2005; 25:11577–11585. [PubMed: 16354915]

26. Sobkowicz HM, Rose JE, Scott GE, Slapnick SM. Ribbon synapses in the developing intact and cultured organ of Corti in the mouse. J. Neurosci. 1982; 2:942–957. [PubMed: 7097321]

27. Dallos P. The active cochlea. J. Neurosci. 1992; 12:4575–4585. [PubMed: 1464757]

28. Knirsch M. Persistence of $Ca_V1.3$ Ca^{2+} channels in mature outer hair cells supports outer hair cell afferent signaling. J. Neurosci. 2007; 27:6442–6451. [PubMed: 17567805]

29. Johnson SL, Adelman JP, Marcotti W. Genetic deletion of SK2 channels in mouse inner hair cells prevents the developmental linearization in the Ca^{2+} dependence of exocytosis. J. Physiol. (Lond.). 2007; 583:631–646. [PubMed: 17627990]

30. Dulon D, Safieddine S, Jones SM, Petit C. Otoferlin is critical for a highly sensitive and linear calcium-dependent exocytosis at vestibular hair cell ribbon synapses. J. Neurosci. 2009; 29:10474–10487. [PubMed: 19710301]

31. Shin OH, Xu J, Rizo J, Südhof TC. Differential but convergent functions of Ca^{2+} binding to synaptotagmin-1 C2 domains mediate neurotransmitter release. Proc. Natl. Acad. Sci. USA. 2009; 106:16469–16474. [PubMed: 19805322]

32. Vician L, et al. Synaptotagmin IV is an immediate early gene induced by depolarization in PC12 cells and in brain. Proc. Natl. Acad. Sci. USA. 1995; 92:2164–2168. [PubMed: 7892240]

33. Ting JT, Kelley BG, Sullivan JM. Synaptotagmin IV does not alter excitatory fast synaptic transmission or fusion pore kinetics in mammalian CNS neurons. J. Neurosci. 2006; 26:372–380. [PubMed: 16407532]

34. Murphy GJ, Glickfeld LL, Balsen Z, Isaacson JS. Sensory neuron signaling to the brain: properties of transmitter release from olfactory nerve terminals. J. Neurosci. 2004; 24:3023–3030. [PubMed: 15044541]

35. Zhang Z, Bhalla A, Dean C, Chapman ER, Jackson MB. Synaptotagmin IV: a multifunctional regulator of peptidergic nerve terminals. Nat. Neurosci. 2009; 12:163–171. [PubMed: 19136969]

36. Wang C-T, et al. Different domains of synaptotagmin control the choice between kiss-and-run and full fusion. Nature. 2003; 424:943–947. [PubMed: 12931189]

37. Mackler JM, Drummond JA, Loewen CA, Robinson IM, Reist NE. The C(2)B Ca^{2+}-binding motif of synaptotagmin is required for synaptic transmission *in vivo*. Nature. 2002; 418:340–344. [PubMed: 12110842]

38. Geppert M, et al. Synaptotagmin I: a major Ca^{2+} sensor for transmitter release at a central synapse. Cell. 1994; 79:717–727. [PubMed: 7954835]

39. Pang ZP, et al. Synaptotagmin-2 is essential for survival and contributes to Ca^{2+} triggering of neurotransmitter release in central and neuromuscular synapses. J. Neurosci. 2006; 26:13493–13504. [PubMed: 17192432]

40. Littleton JT, Stern M, Perin M, Bellen HJ. Calcium dependence of neurotransmitter release and rate of spontaneous vesicle fusions are altered in *Drosophila* synaptotagmin mutants. Proc. Natl. Acad. Sci. USA. 1994; 91:10888–10892. [PubMed: 7971978]

41. Chapman ER, Desai RC, Davis AF, Tornehl CK. Delineation of the oligomerization, AP-2 binding and synprint binding region of the C2B domain of synaptotagmin. J. Biol. Chem. 1998; 273:32966–32972. [PubMed: 9830048]

42. Thomas DM, Ferguson GD, Herschman HR, Elferink LA. Functional and biochemical analysis of the C2 domains of synaptotagmin IV. Mol. Biol. Cell. 1999; 10:2285–2295. [PubMed: 10397765]

43. Stevens CF, Sullivan JM. The synaptotagmin C2A domain is part of the calcium sensor controlling fast synaptic transmission. Neuron. 2003; 39:299–308. [PubMed: 12873386]

44. Nagy G, et al. Different effects on fast exocytosis induced by synaptotagmin 1 and 2 isoforms and abundance but not by phosphorylation. J. Neurosci. 2006; 26:632–643. [PubMed: 16407561]

45. Xu J, Mashimo T, Südhof TC. Synaptotagmin-1, -2 and -9: Ca^{2+} sensors for fast release that specify distinct presynaptic properties in subsets of neurons. Neuron. 2007; 54:567–581. [PubMed: 17521570]

46. Moody WJ, Bosma MM. Ion channel development, spontaneous activity, and activity-dependent development in nerve and muscle cells. Physiol. Rev. 2005; 85:883–941. [PubMed: 15987798]

47. Gu X, Spitzer NC. Distinct aspects of neuronal differentiation encoded by frequency of spontaneous Ca^{2+} transients. Nature. 1995; 375:784–787. [PubMed: 7596410]

48. Marcotti W, Johnson SL, Holley MC, Kros CJ. Developmental changes in the expression of potassium currents of embryonic, neonatal and mature mouse inner hair cells. J. Physiol. (Lond.). 2003; 548:383–400. [PubMed: 12588897]
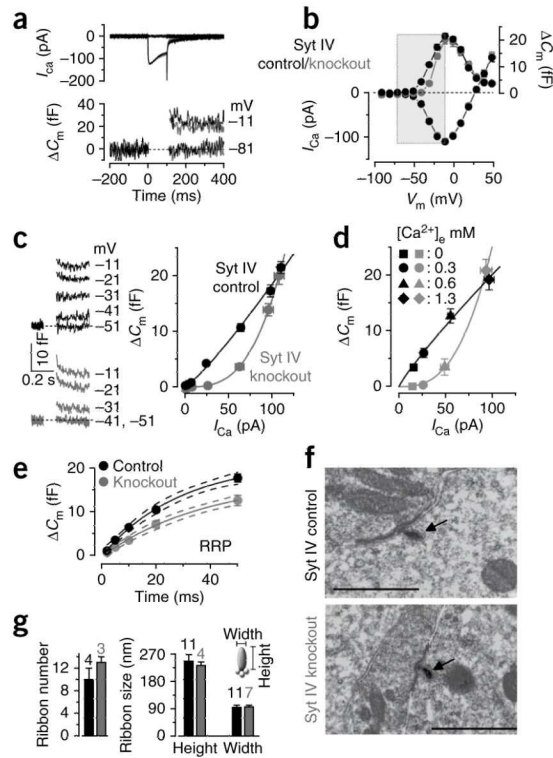
Figure 1.
Exocytotic Ca^{2+} dependence and ribbon morphology in control and knockout adult Syt IV IHCs. (**a**,**b**) I_{Ca} and ΔC_m from P18–36 IHCs in response to 100-ms voltage steps (10-mV increments) from −81 mV using 1.3 mM extracellular Ca^{2+}. In **a**, only peak responses and those at −81 mV are shown for clarity. (**c**) Exocytotic Ca^{2+} dependence was abnormal in knockout IHCs. The synaptic transfer curves (right) were obtained by plotting ΔC_m against I_{Ca} between −71 mV and −11 mV (shaded area in **b**). Fits were made according to equation (1) (Online Methods). Left, average ΔC_m traces from all 27 control and 28 knockout IHCs. (**d**) Synaptic transfer curves (fitted using equation (1)) obtained by plotting the maximal I_{Ca} and ΔC_m values while superfusing IHCs (P21–36) with different extracellular $[Ca^{2+}]$ (0, 0.3, 0.6 and 1.3 mM). The number of measurements taken at each $[Ca^{2+}]$ were 7, 6, 6 and 13 (control, black) and 9, 8, 7 and 13 (knockout, gray). (**e**) Rate of vesicle fusion in adult control (P18–20) and knockout (P20–28) IHCs (see Online Methods for details). Dotted lines represent 95% confidence intervals for the single exponential fits. RRP, readily releasable pool. (**f**) TEM showing typical cross-sectional profiles of ribbons from a control and a Syt IV knockout P26 IHC. Scale bar represents 1 μm. (**g**) Histogram showing that the number (left) and shape (height and width, right) of ribbons was similar between control and knockout IHCs. Error bars indicate s.e.m.
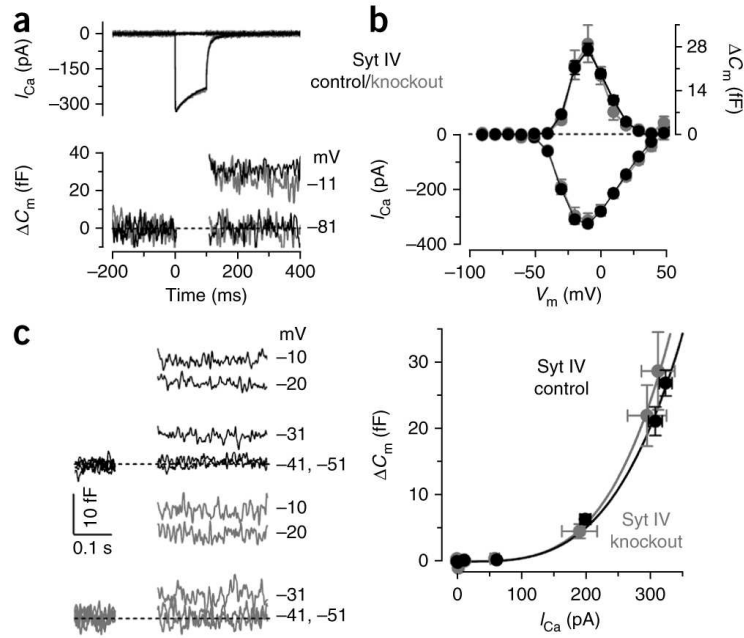
Figure 2.
Synaptotagmin IV has no role at immature IHC ribbon synapses. (**a**) I_{Ca} and ΔC_m recordings in immature Syt IV knockout IHCs. (**b**) The maximal size of I_{Ca} and ΔC_m was -324 ± 10 pA and 27 ± 2 fF in control IHCs ($n = 20$) and -312 ± 26 pA and 29 ± 6 fF in knockout cells ($n = 7$). (**c**) Right, the synaptic transfer curves (obtained as described in Fig. 1c). The ΔC_m traces shown on the left are averages from 20 control and 7 Syt IV knockout IHCs and indicate that ΔC_m responses were observed from around -31 mV. Exocytotic Ca^{2+} dependence in knockout immature IHCs was similar to control cells and the power N values from fits to all individual cells using equation (1) were 3.3 ± 0.2 (control) and 3.3 ± 0.3 (knockout).
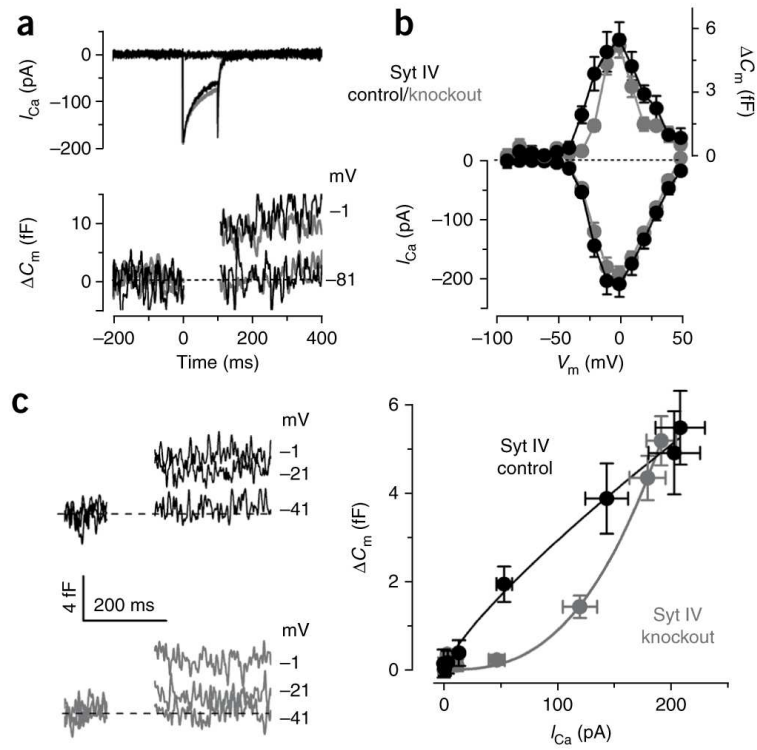
Figure 3.
Role of synaptotagmin IV at immature OHC ribbon synapses. (**a**) I_{Ca} and ΔC_m responses recorded from OHCs (P3–4) using the same protocol described in Figure 1a, but in 5 mM extracellular Ca^{2+}. (**b**) Control and Syt IV knockout cells had similar maximal I_{Ca} (control, -207 ± 22 pA, $n = 7$; knockout, -191 ± 13 pA, $n = 13$) and ΔC_m (control, 5.5 ± 0.8 fF; knockout, 5.2 ± 0.6 fF), as shown by the I_{Ca}-V and ΔC_m-V curves. (**c**) Synaptic transfer curves (obtained as described in Fig. 1c) were abnormal in Syt IV knockout OHCs. The power N values from fits to all individual cells were 0.9 ± 0.2 (control) and 3.0 ± 0.3 (knockout). ΔC_m traces shown on the left are averages from all 7 control and 13 Syt IV knockout OHCs.

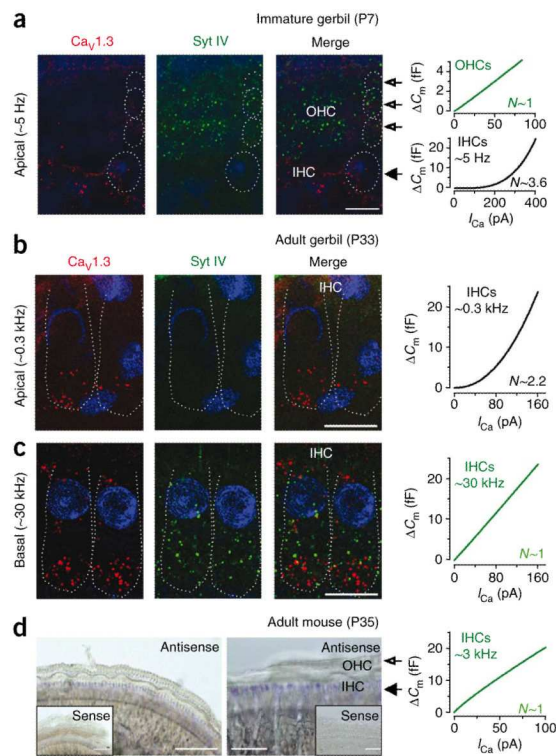**Figure 4.**
Syt IV expression in the gerbil and mouse cochlea. (**a**) Immunostaining of Ca$_V$1.3 and Syt IV proteins in the apical region of the immature (P7) gerbil cochlea. Syt IV was present in OHCs, but not in IHCs (merged image). Scale bar represents 10 μm. Hair-cell boundaries are outlined in the merged image. DAPI staining is shown in blue. Right panels in **a–d** give an indication of the characteristic exocytotic Ca^{2+} dependence in immature (**a**) and adult (**b,c**) gerbil and mouse (**d**) hair cells (lines shown are fits from data shown in refs. 12,9 and Fig. 1, respectively). (**b,c**) Immunostaining of Syt IV and Ca$_V$1.3 Ca^{2+} channels in apical and basal IHCs of the adult (P33) gerbil cochlea, with basal cells showing staining for both proteins and apical cells showing staining for just Ca$_V$1.3 (see merged images). Images show only staining of maximum intensity projections over all layers of the *z* stack after deconvolution. Scale bars represent 10 μm. Staining was absent in control experiments on adult basal-coil IHCs, where both Syt IV and Ca$_V$1.3 antibodies were omitted (data not shown). (**d**) *In situ* hybridization showing the expression of *Syt4* mRNA at the IHC level in P35 mouse cochleae (middle panel represents an expanded version of the left panel). Scale bars represent 200 μm (left) and 50 μm (middle). Note that in gerbil and mouse hair cells, the expression of Syt IV was associated with linear exocytotic Ca^{2+} dependence.
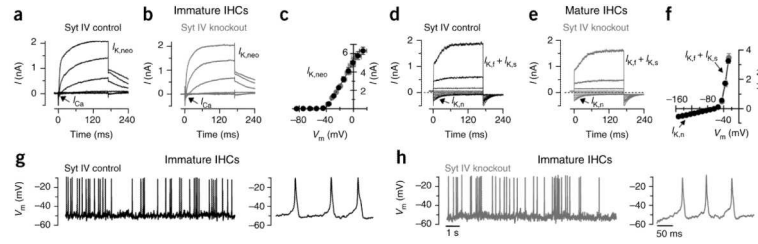
Figure 5.
Electrical properties of IHCs from Syt IV mice. (**a,b**) Current recordings from a control (**a**) and a knockout (**b**) immature IHC. Membrane currents elicited from immature P5 IHCs by depolarizing voltage steps (10-mV nominal increments) from −84 mV. The outward K$^+$ current $I_{K,neo}$ (ref. 48) appeared to be normal. (**c**) The control and knockout IHCs had similar average steady-state current-voltage (*I*-*V*) curves (controls, $n = 8$; knockouts, $n = 6$). (**d,e**) Currents elicited in adult IHCs by depolarizing voltage steps from −164 mV from the holding potential of −64 mV. All three of the K$^+$ currents characteristic of adult IHCs ($I_{K,s}$, $I_{K,n}$ and $I_{K,f}$[48]) appeared to be normal. (**f**) Average steady-state *I*-*V* curves. The number of IHCs investigated was 7 for both control (P28) and knockout (P29) mice. (**g,h**) Spontaneous action potential activity recorded from knockout immature P5 IHCs was similar to that of control littermates and to that previously reported in age-matched cells[29]. Right, action potentials on an expanded time scale.
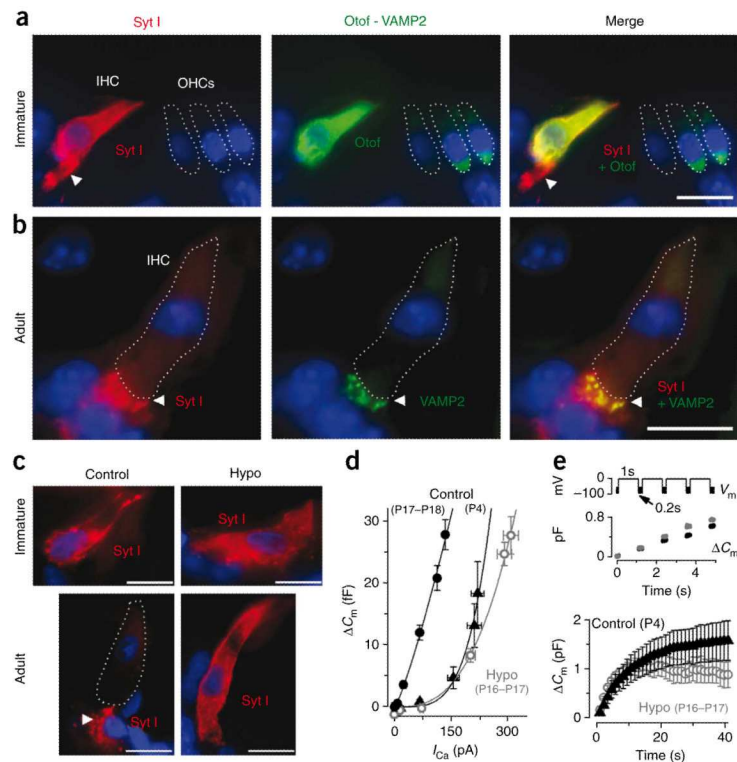
Figure 6.
Synaptotagmin I is expressed in cochlear IHCs. (**a**) In immature mice, the Syt I antibody stained IHCs (red), as indicated by its colocalization with the hair-cell marker otoferlin (green). Syt I was also present in the efferent nerve terminals below the IHCs (arrowheads). The otoferlin antibody also stained immature OHCs. (**b**) In adult mice, Syt I only stained the efferent terminals (arrowheads) and colocalized with VAMP2, a marker for efferents[15] (green). (**c**) Syt I antibody staining in control immature (P7) and adult (P19) rat IHCs was the same as that observed in normal mice (see above). Both immature and adult IHCs from hypothyroid (Hypo) rats, which do not express otoferlin[18], expressed Syt I. Scale bars in **a–c** represent 10 μm. DAPI staining is shown in blue. (**d**) Exocytotic Ca^{2+} dependence was normal (linear) in adult controls, but was high order in hypothyroid rat IHCs, which was similar to that measured in immature cells. Fits are according to equation (1). The average power N values from fits to all individual cells were 4.1 ± 0.3 (immature control, $n = 4$), 1.2 ± 0.1 (adult control, $n = 10$) and 3.1 ± 0.2 (adult hypothyroid, $n = 10$). (**e**) ΔC_m responses from immature control ($n = 3$) and adult hypothyroid ($n = 3$) rat IHCs elicited using 1-s repetitive voltage steps to −11 mV (top, interstep interval of 200 ms). For clarity, only the first few ΔC_m responses are shown (middle). Average cumulative ΔC_m values are shown in the bottom panel.
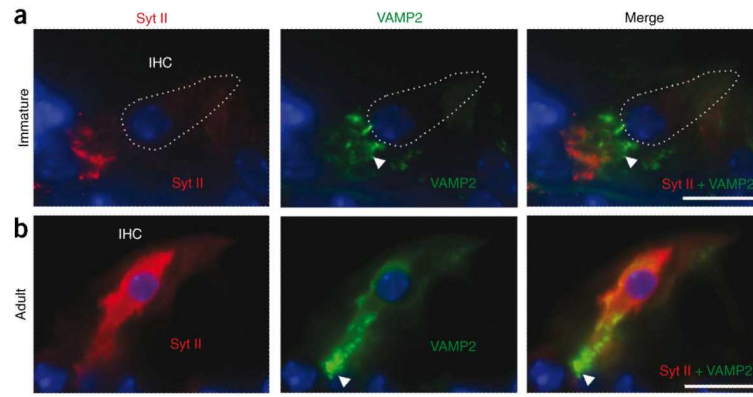
Figure 7.
Distribution of synaptotagmin II in immature and adult IHCs. (**a**) In immature mice, the Syt II antibody, which recognizes a distinct Syt II specific protein sequence at the cytoplasmic domain, stained efferent nerve fibers (red), as indicated by its localization below VAMP2 (green, arrowhead). (**b**) In adult animals, Syt II stained the IHC (red) and we detected very little colocalization with VAMP2 (green, arrowhead). Scale bars represent 10 μm. DAPI staining is shown in blue.